

Quantum-aware Transformer model for state classification

Przemysław Sekuła^{1,2}[0000-0002-4599-1077], Michał
 Romaszewski¹[0000-0002-8227-929X], Przemysław
 Głomb¹[0000-0002-0215-4674], Michał Cholewa¹[0000-0001-6549-1590], and
 Łukasz Paweł¹[0000-0002-0476-7132]

¹ Institute of Theoretical and Applied Informatics, Polish Academy of Sciences,
 Bałtycka 5, 44-100 Gliwice, Poland

² University of Maryland, College Park, Department of Civil and Environmental
 Engineering, MD, USA
 {psekula,mromaszewski,przemg,mcholewa,lpawela}@iitis.pl

Abstract. Entanglement is a fundamental feature of quantum mechanics, playing a crucial role in quantum information processing. However, classifying entangled states, particularly in the mixed-state regime, remains a challenging problem, especially as system dimensions increase. In this work, we focus on bipartite quantum states and present a data-driven approach to entanglement classification using transformer-based neural networks. Our dataset consists of a diverse set of bipartite states, including pure separable states, Werner entangled states, general entangled states, and maximally entangled states. We pretrain the transformer in an unsupervised fashion by masking elements of vectorized Hermitian matrix representations of quantum states, allowing the model to learn structural properties of quantum density matrices. This approach enables the model to generalize entanglement characteristics across different classes of states. Once trained, our method achieves near-perfect classification accuracy, effectively distinguishing between separable and entangled states. Compared to previous Machine Learning, our method successfully adapts transformers for quantum state analysis, demonstrating their ability to systematically identify entanglement in bipartite systems. These results highlight the potential of modern machine learning techniques in automating entanglement detection and classification, bridging the gap between quantum information theory and artificial intelligence.

Keywords: Quantum entanglement · State classification · Transformers · Large language models

1 Introduction

The entanglement phenomenon is at the heart of quantum information, enabling its key applications such as quantum computing, secure communication,

and enhanced metrology. Unlike classical correlations, entanglement represents a uniquely quantum feature where the state of a system cannot be described independently of its subsystems. This fundamental property underlies protocols like quantum teleportation, superdense coding, and quantum key distribution, as well as quantum computational speedups [25,17]. However, not all quantum states exhibit entanglement, and distinguishing entangled states from separable ones is a crucial yet challenging problem in quantum information science. The ability to efficiently classify quantum states has direct implications for the practical implementation of quantum technologies, motivating the development of reliable entanglement detection and classification methods.

Bipartite quantum states, which describe systems naturally partitioned into two subsystems, are fundamental in quantum information science and serve as a basis for studying quantum correlations and computational advantages. These states reside in a tensor product space $L(\mathbb{C}^{d_1} \otimes \mathbb{C}^{d_2})$, where entanglement emerges as a crucial resource for various quantum information applications [14,6], such as secure communication, quantum-enhanced computation, and efficient information transfer. For pure bipartite states, i.e., vectors in $\mathbb{C}^{d_1} \otimes \mathbb{C}^{d_2}$, entanglement can be clearly identified: a state is separable if and only if it can be expressed as a tensor product of subsystem states. Any departure from this structure signifies entanglement, which directly influences quantum nonlocality, measurement-based quantum computing, and the efficiency of entanglement-assisted protocols.

The identification of entanglement for bipartite states is straightforward in the case of pure states but becomes significantly more challenging when considering mixed bipartite states. A variety of analytical and numerical methods have been developed for the characterization and detection of mixed-state entanglement. One of the most celebrated approaches is based on the *positivity of the partial transpose (PPT)*, introduced by Peres [19] and Horodecki [11]. While the PPT criterion is both necessary and sufficient for separability in low-dimensional cases ($\mathbb{C}^2 \otimes \mathbb{C}^2$ and $\mathbb{C}^2 \otimes \mathbb{C}^3$), in higher dimensions, a state can be *PPT and still entangled*. Such states are known as *bound entangled* states [12] (see Fig. 1 for sketch). They cannot be distilled into pure entangled states using local operations and classical communication (LOCC), rendering them entangled yet practically “inaccessible” for certain quantum information protocols [1]. This discovery highlighted the limitations of the PPT criterion and the intricate nature of entanglement in higher-dimensional systems. To emphasize this difference, entangled states which are not bound entangled are sometimes called free entangled states.

To address these limitations, other techniques—particularly *entanglement witnesses*—have been introduced [14,10]. An entanglement witness is a Hermitian operator W with the property that $\text{Tr}(W \rho_{\text{sep}}) \geq 0$ for all separable states ρ_{sep} , but $\text{Tr}(W \rho_{\text{ent}}) < 0$ for at least one entangled state ρ_{ent} . Finding and optimizing entanglement witnesses can often be formulated via semidefinite programming techniques, and in many cases, witnesses can be tailored to detect specific classes of entangled states, including those exhibiting bound entanglement. Additional approaches to mixed-state entanglement include various *entan-*

glement measures (e.g., negativity, entanglement of formation), which attempts to quantify the degree of entanglement in a given density operator [24,20].

Another class of approaches relies on machine learning (ML) to identify entanglement directly from the data. In [8], authors use automated ML for state classification. Instead of directly measuring entanglement properties, the state is reconstructed, and entanglement is inferred from the data itself. Recently, Transformers have also been applied to quantum random number validation [7], showcasing their ability to handle large input sequences efficiently and perform multiple statistical tests in parallel. The same self-attention mechanism that captures subtle global dependencies in random bit streams can likewise model the intricate correlations of bipartite quantum states, suggesting that Transformers are a promising architecture for entanglement classification under partial or noisy data.

Despite significant progress, a complete classification of bipartite entangled mixed states remains an open challenge, particularly as system dimensions grow. In this work, we take a data-driven approach to this problem by generating a diverse dataset of pure and mixed states through multiple methods and employing transformer-based neural networks to analyze their properties and classify them. We demonstrate that entanglement identification can be performed effectively from the data itself, extending the range of successful classification beyond previous studies. Furthermore, we validate the application of transformer architectures in this domain, achieving a breakthrough where prior deep learning approaches [8] have struggled. By integrating machine learning with established theoretical criteria, we provide a scalable framework for systematically detecting and categorizing entanglement, bridging the gap between quantum information theory and modern Artificial Intelligence techniques.

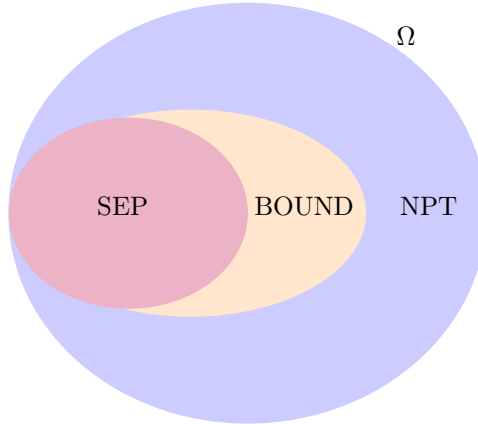


Fig. 1. Schematic representation of the set of mixed quantum states Ω depicting separable states (SEP) ρ_{sep} , bound entangled states (BOUND) σ_{bound} and negative partial transpose states (NPT) ξ_{npt} .

This paper is organized as follows. In Section 2, we explain the methodology for constructing our dataset. In Section 3, we detail our proposition of the Quantum-aware Transformer model and its training scheme. In Section 4, we present the results of validation experiments and discussion.

The code for this paper is publicly available on GitHub³ under an open license to facilitate result reproducibility and transparency and the data can be shared upon a reasonable request.

2 Dataset generation

Quantum states, the basic objects of quantum mechanics, can be broadly classified as *pure* or *mixed*. A *pure state* is described by a single d -dimensional vector $|\psi\rangle$ in a complex Euclidean space \mathbb{C}^d , and a corresponding density operator $\rho = |\psi\rangle\langle\psi|$. This operator satisfies $\rho^2 = \rho$ and $\text{Tr}(\rho) = 1$. When $d = 2$, the corresponding system is called a qubit; for $d = 3$, it is called a qutrit.

In contrast, a *mixed state* is represented by a statistical ensemble of pure states, described by a density operator $L(\mathbb{C}^d) \ni \rho = \sum_i p_i |\psi_i\rangle\langle\psi_i|$, where $p_i \in [0, 1]$ and $\sum_i p_i = 1$ [16]. Such states often emerge from partial traces of larger systems or incomplete information about the quantum system under study. Note that ρ is a positive semidefinite matrix.

In many quantum information scenarios, one focuses on *bipartite* states. These describe a physical system that can be naturally partitioned into two subsystems, $|\psi\rangle \otimes |\phi\rangle$, associated with complex Euclidean spaces \mathbb{C}^{d_1} and \mathbb{C}^{d_2} . The total state then lives in the tensor product space $\mathbb{C}^{d_1} \otimes \mathbb{C}^{d_2}$. Bipartite quantum systems are not only a cornerstone for foundational studies of quantum correlations but also play a central role in key quantum information tasks such as quantum teleportation, quantum key distribution, and superdense coding.

For *pure bipartite states*, there exists a straightforward way to distinguish entangled from separable states: a pure bipartite state $|\psi\rangle \in \mathbb{C}^{d_1} \otimes \mathbb{C}^{d_2}$ is separable if and only if it can be written as $|\xi\rangle = |\psi\rangle \otimes |\phi\rangle$. Any deviation from this product structure indicates entanglement.

In this work, we study the following cases of discrimination between separable and entangled states:

1. two-qubit states, $\mathbb{C}^2 \otimes \mathbb{C}^2$,
2. qubit-qutrit systems, $\mathbb{C}^2 \otimes \mathbb{C}^3$,
3. qutrit-qutrit systems, $\mathbb{C}^3 \otimes \mathbb{C}^3$,

For each of these, we generate a dataset consisting of:

1. pure separable states,
2. general entangled states,
3. Werner entangled states (for qubit-qubit and qutrit-qutrit systems),
4. maximally entangled states (for qubit-qubit and qutrit-qutrit systems),

³ <https://github.com/iitis/LQM>

5. bound entangled states from the family by Horodecki [13] (for qutrit-qutrit systems).

For this work we assume we have access to the full tomography [3] of each ρ , hence we encode each state as a vector of $2d_1d_2$ real variables.

The details of the sampling are described in the following subsections. Uniform sampling of quantum states (either pure or mixed) was conducted utilizing the QuantumInformation.jl package [5].

2.1 Sampling pure separable states

In this case, we need to sample uniformly normalized vectors of the form $\mathbb{C}^{d_1} \otimes \mathbb{C}^{d_2} \ni |\psi\rangle = |\phi_1\rangle \otimes |\phi_2\rangle$. This is done in the following steps:

1. Sample a non-normalized $|x\rangle \in \mathbb{C}^{d_1}$ with each element x_i such that $\text{Re}(x_i) \sim N(0, 1)$ and $\text{Im}(x_i) \sim N(0, 1)$.
2. Normalize $|x\rangle$: $|\phi_1\rangle = \frac{|x\rangle}{\| |x\rangle \|}$.
3. Repeat steps 1 and 2 to obtain $|\phi_2\rangle$.
4. Put $|\psi\rangle = |\phi_1\rangle \otimes |\phi_2\rangle$.

This procedure ensures that each $|\phi_i\rangle$ is sampled from the Haar measure.

2.2 Sampling Werner entangled states

A Werner state is a mixed state having the form

$$\rho_{\text{wer}} = (1 - p) |\psi\rangle\langle\psi| + p\rho^*, \quad (1)$$

where ρ^* is the maximally mixed state

$$\rho^* = \frac{\mathbb{1}}{d^2} \quad (2)$$

and

$$|\psi\rangle = \frac{1}{\sqrt{d}} \sum_{i=0}^{d-1} |ii\rangle. \quad (3)$$

It can be shown that the state remain entangled for

$$p < \frac{d}{d+1}. \quad (4)$$

We sample p uniformly in this interval and construct ρ_{wer} .

2.3 Sampling general entangled states

We sample general entangled states by uniformly sampling the state of all mixed quantum states and only accepting the state as entangled when it is NPT. The steps are:

1. Sample a square Ginibre matrix, G , of dimension $d_1 d_2$. Elements G_{ij} pertain to the complex normal distribution $\text{Re}(G_{ij}) \sim N(0, 1)$ and $\text{Im}(G_{ij}) \sim N(0, 1)$.
2. Calculate $W = GG^\dagger$.
3. Normalize the trace, $\rho = \frac{W}{\text{Tr} W}$.
4. Check the Peres-Horodecki criterion. If ρ is NPT, accept it into the set; otherwise, repeat the procedure.

Note that this procedure is quite efficient, especially as the dimension increases, as the relative volume of the separable states diminishes [26,27,28].

2.4 Sampling maximally entangled states

We sample maximally entangled states by sampling unitary matrices, vectorizing them, and renormalizing them [21]. The procedure is:

1. Sample a square Ginibre matrix G of dimension d as described in Section 2.3.
2. Calculate its QR decomposition $G = QR$, where Q is a unitary matrix and R is upper triangular.
3. Multiply i -th column of Q , Q_i , by the phase of the corresponding diagonal element of R , R_{ii} , thus obtaining the i -th column of a unitary matrix U . This step is necessary to ensure the proper distribution of eigenvalues of U [15,18].
4. Vectorize the matrix U and normalize by $\frac{1}{\sqrt{d}}$.

2.5 Sampling bound entangled states

This procedure is based on a family of bound entangled states described in [13]. First, let us introduce

$$\begin{aligned}\sigma_+ &= \frac{1}{3} (|01\rangle\langle 01| + |12\rangle\langle 12| + |20\rangle\langle 20|) \\ \sigma_- &= \frac{1}{3} (|10\rangle\langle 10| + |21\rangle\langle 21| + |02\rangle\langle 02|) \\ |\psi\rangle &= \frac{1}{\sqrt{3}} (|00\rangle + |11\rangle + |22\rangle).\end{aligned}\tag{5}$$

We construct a state ρ as follows

$$\rho_\alpha = \frac{2}{7} |\psi\rangle\langle\psi| + \frac{\alpha}{7} \sigma_+ + \frac{5-\alpha}{7} \sigma_-.\tag{6}$$

Depending on parameter α this state can be separable ($2 \leq \alpha \leq 3$), bound entangled ($3 < \alpha \leq 4$) or free entangled ($4 < \alpha \leq 5$). Hence, we sample α uniformly in the range $(3, 4]$.

3 Quantum-aware Transformer model

We use a Transformer [23] based model for processing quantum state matrices, leveraging its self-attention mechanism for structured data reconstruction. Transformers, originally designed for language sequence modeling, operate on sets of input tokens with global context awareness. Here, we treat quantum state matrices as tokenized inputs, where each matrix element (real and imaginary parts) forms a structured sequence. By applying a masked autoencoding strategy, we train the model to reconstruct missing matrix elements, allowing it to learn intrinsic quantum state properties. This approach enables the Transformer to capture patterns in quantum data and improve downstream tasks like entanglement classification.

3.1 Model Description

We employ a masked Transformer architecture, referred to as the *MaskedTransformer*, to reconstruct partially masked 2D quantum data. The input is first flattened from $[B, 2N^2]$ into $[B, N^2, 2]$, where B stands for the size of data batch, N is the size of the original square matrix (each entry contains real and imaginary parts). Tokens in this representation are randomly masked and replaced by a *mask token*, and the partially masked sequence is passed through a Transformer encoder composed of multi-head self-attention layers and feed-forward networks.

Each token embedding is further augmented with a trainable positional vector \mathbf{p}_i , ensuring that the Transformer retains the relative location of each matrix element in the spatial grid. Concretely, we added $\mathbf{p}_i \in \mathbb{R}^d$ to the embedded token \mathbf{x}_i , yielding

$$\tilde{\mathbf{x}}_i = \text{Embed}(\mathbf{x}_i) + \mathbf{p}_i, \quad (7)$$

where Embed is the token embedding function. This positional encoding is crucial to provide the necessary positional information for the self-attention mechanism.

A simple linear decoder projects the final encoded representations back to real and imaginary components, reconstructing both the originally masked and unmasked portions. This masked-reconstruction approach is analogous to masked autoencoders or BERT [4] like masking methods, thereby encouraging the model to infer missing entries from the surrounding context.

In our experiments, we tested three configurations corresponding to $n = 4$ (for $\mathbb{C}^2 \otimes \mathbb{C}^2$), $n = 6$ (for $\mathbb{C}^2 \otimes \mathbb{C}^3$), and $n = 9$ (for $\mathbb{C}^3 \otimes \mathbb{C}^3$). All other Transformer hyperparameters (embedding dimension, number of attention heads, number of layers, and dropout) were selected during the initial research phase by trial-and-error method, and remained the same across these experiments.

We used separate datasets for each experiment for pretraining and classification, as presented in Table 1. In every experiment, the dataset was divided into training, validation, and test subsets. The validation evaluation was performed every epoch, and the test evaluation was performed after the training was completed.

Group name	$\mathbb{C}^2 \otimes \mathbb{C}^2$	Pretraining		Classification		
		$\mathbb{C}^2 \otimes \mathbb{C}^3$	$\mathbb{C}^3 \otimes \mathbb{C}^3$	$\mathbb{C}^2 \otimes \mathbb{C}^2$	$\mathbb{C}^2 \otimes \mathbb{C}^3$	$\mathbb{C}^3 \otimes \mathbb{C}^3$
sep	4,000,000	8,000,000	6,000,000	1,000,000	1,000,000	1,000,000
general-ent	2,000,000	8,000,000	2,000,000	300,000	1,000,000	500,000
werner-ent	2,000,000		2,000,000	300,000		500,000
max-ent	2,000,000		2,000,000	300,000		500,000
horodecki-bound			2,000,000			500,000
horodecki-ent			2,000,000			500,000

Table 1. Training data sizes for Pretraining and Classifier tasks. Numbers indicate samples used for each model configuration and data type. Group names correspond to the type of data (pure separable, general entangled etc.) described in Section 2.

3.2 Pretraining

In this stage, we train the *MaskedTransformer* from scratch as an autoencoder. Specifically, we:

- Use the datasets of 10 mln (for $\mathbb{C}^2 \otimes \mathbb{C}^2$) and 16 mln ($\mathbb{C}^2 \otimes \mathbb{C}^3$ and $\mathbb{C}^3 \otimes \mathbb{C}^3$), described in detail in Table 1 in the *Pretraining* columns.
- Split the dataset it into training (90%), validation (5%), and test (5%) partitions.
- Randomly mask a given fraction (15%) of tokens, replacing them with a learned mask token.
- Pass the masked tokens through the Transformer encoder and reconstruct them via a linear decoder head.
- Optimize the full reconstruction loss using mean squared error (MSE).

The training uses a well-known cosine-annealing learning rate schedule and standard PyTorch Lightning callbacks for logging and checkpointing. Upon completion, the final checkpoints were saved for subsequent classification.

To evaluate the pretraining performance we introduce a metric called Hermitian distance, that measures the deviation of a matrix from being perfectly Hermitian by computing the average Frobenius norm of the difference between the matrix and its conjugate transpose:

$$h = \frac{1}{b} \sum_{k=1}^b \sqrt{\|\mathbf{A}_k - \mathbf{A}_k^\dagger\|_F}, \quad (8)$$

where b is the number of matrices in the batch, and \mathbf{A}_k denotes the k -th complex matrix. The notation \mathbf{A}_k^\dagger refers to its conjugate transpose, and $\|\cdot\|_F$ indicates the Frobenius norm. For a Hermitian matrix, $\mathbf{A}_k = \mathbf{A}_k^\dagger$, which makes the norm vanish. When the matrix is split into real and imaginary parts, $\mathbf{A}_k = \mathbf{R}_k + i\mathbf{I}_k$, Hermiticity requires \mathbf{R}_k to be symmetric ($\mathbf{R}_k = \mathbf{R}_k^T$) and \mathbf{I}_k to be anti-symmetric ($\mathbf{I}_k = -\mathbf{I}_k^T$). Consequently, the quantity $\mathbf{A}_k - \mathbf{A}_k^\dagger$ captures deviations from these symmetries, and its Frobenius norm measures how far the matrix is

from being perfectly Hermitian. Averaging over all matrices in the batch yields the final distance h .

We used this metric to evaluate our pretraining process by assessing how well the pretrained model preserves the Hermitian structure of the data when 15% of the matrix is reconstructed by a network. A lower Hermitian distance indicates that the intrinsic mathematical properties are maintained, serving as a meaningful indicator of the quality of pretraining.

3.3 Classifier Training

After pretraining, we fine-tune or adapt the learned Transformer weights for a downstream binary classification task. The core steps are:

- Load the pre-trained Transformer weights into a new model that augments the Transformer encoder with a feed-forward classification head (two-class output).
- Use the datasets of 1.9 mln (for $\mathbb{C}^2 \otimes \mathbb{C}^2$), 2 mln (for $\mathbb{C}^2 \otimes \mathbb{C}^3$), and 3.5 mln (for $\mathbb{C}^3 \otimes \mathbb{C}^3$), described in detail in Table 1 in the *Classification* subsection. This data is separate from the pretraining data.
- Split the dataset into training (90%), validation (5%), and test (5%) partitions.
- Train the network using cross-entropy loss and the same PyTorch Lightning setup, with logging, checkpointing, and cosine-annealing learning rate schedule.

This two-stage approach leverages the pre-trained Transformer’s learned representation of the quantum matrices, enhancing the performance of the downstream classification task.

4 Results and discussion

To determine the final results of the pretraining and classification, we used the separate data subset that was not used during the training phase neither for training nor for validation and testing. This subset comprises of 100,000 samples for each of the classes. The final evaluation was carried out for both pretraining and classification after the entire training process was completed.

Pretraining During the pretraining phase, both the loss function and the Hermitian distance improved significantly. Table 2 shows the averaged results of the Hermitian distance metric for the pretraining phase. The results are consistent and show that, overall, the pretraining process ended up generating models that are able to reconstruct the Hermitian structure of the data. Surprisingly, the Hermitian distances achieved very low values during the early pretraining. We did not observe any significant improvement in this metric after the first few epochs, whereas the loss function continued to decrease. This suggests that the model learned the Hermitian structure of the data very quickly, and the loss function was optimized to a greater extent.

Group name	Untrained			Pretrained		
	$\mathbb{C}^2 \otimes \mathbb{C}^2$	$\mathbb{C}^2 \otimes \mathbb{C}^3$	$\mathbb{C}^3 \otimes \mathbb{C}^3$	$\mathbb{C}^2 \otimes \mathbb{C}^2$	$\mathbb{C}^2 \otimes \mathbb{C}^3$	$\mathbb{C}^3 \otimes \mathbb{C}^3$
sep	6.686	3.718	8.101	0.265	0.364	0.419
general-ent	6.704	3.716	8.098	0.189	0.187	0.167
werner-ent	6.645		8.131	0.183		0.222
max-ent	6.693		8.102	0.296		0.449
horodecki-bound			8.104			0.120
horodecki-ent			8.102			0.122

Table 2. Averaged Hermitian distances for untrained, and fully pretrained models.

Classification The classification results are presented in Table 3. It is important to emphasize that, while results are presented for each type of state, the classification was deliberately kept binary—entangled vs. separable—as this is the relevant distinction for practical applications. The results show that the model was able to classify the states with very high accuracy. The results are consistent across all dimensions and classes. The only errors appear for the pure separable states $\mathbb{C}^2 \otimes \mathbb{C}^2$ and $\mathbb{C}^2 \otimes \mathbb{C}^3$ groups, where a few of states were misclassified as entangled. This confirms the validity of our approach, as the model effectively captures the structural properties of quantum states and generalizes well across different state classes and dimensions, with only minimal misclassification in specific cases.

Group name	$\mathbb{C}^2 \otimes \mathbb{C}^2$	$\mathbb{C}^2 \otimes \mathbb{C}^3$	$\mathbb{C}^3 \otimes \mathbb{C}^3$
sep	99.995%	99.998%	100%
general-ent	100%	100%	100%
werner-ent	100%		100%
max-ent	100%		100%
horodecki-bound			100%
horodecki-ent			100%

Table 3. Accuracy of binary classification (entangled vs separated) for each data group.

To further verify our results, we tested whether the deep fine-tuning during classification training provides an additional learning benefit beyond the pre-training phase. Specifically, we took a pretrained model and froze all its layers except for the final classification layer, which was then fine-tuned on labeled data. This approach aimed to determine whether the pretrained representations alone were sufficient for entanglement classification or if further adaptation was necessary. The fine-tuned model performed nearly perfectly on $\mathbb{C}^2 \otimes \mathbb{C}^2$ and $\mathbb{C}^2 \otimes \mathbb{C}^3$ states but struggled with $\mathbb{C}^3 \otimes \mathbb{C}^3$ states, achieving around 85% accuracy. A detailed breakdown revealed that while entangled states were consistently classified correctly, the model frequently misclassified separable states. This suggests that

while the pretrained model captures general entanglement patterns, adapting deeper layers during training may be crucial for distinguishing subtle features in higher-dimensional separable states.

Discussion Our work is closely related to [8], which also explores automated entanglement classification. However, we achieve significantly better results, with near-perfect accuracy compared to their reported range of 62–88%. While their approach struggled with deep learning, we successfully adapted transformers into a highly effective classification method. An important distinction is that the presence of bound entangled states in our dataset does not degrade performance. Additionally, our dataset is substantially larger, containing millions of states, whereas theirs consisted of only 3,254. Their dataset generation method, in principle, allows for bound entangled states in any dimension, while our approach focuses on a specific family of states for the $\mathbb{C}^3 \otimes \mathbb{C}^3$ case. However, their generation method is much more computationally expensive. Overall, our results are consistent with theirs, but we extend the approach significantly, demonstrating the feasibility of deep learning for entanglement classification at a much larger scale.

Our work serves as an example of the successful integration of machine learning techniques with quantum information science. Similar approaches—whether in developing quantum information models [2] or solving quantum computing problems [22]—represent a promising direction for the field. We expect that this fusion of computational methods and quantum theory will gain increasing prominence, much like the impact of machine learning in computational chemistry.

Our approach addresses a different but related problem compared to [9]. Their work focuses on generating entanglement witnesses for specific types of quantum states and specially structured witnesses. While their method is well-executed, it is inherently limited, as reflected in their choice of states. In contrast, our approach is applied to a significantly larger dataset, allowing for a broader and more flexible classification of entanglement. However, their method extends to multipartite entanglement, an area we have not yet explored.

Conclusions We have demonstrated that transformer-based neural networks can effectively classify bipartite quantum states as entangled or separable by learning directly from quantum state matrices. By leveraging a masked autoencoding pretraining strategy, our model captures the structural properties of density matrices, achieving near-perfect classification accuracy across various state types and dimensions. These results highlight the potential of modern deep learning architectures for quantum information processing, paving the way for scalable, data-driven approaches to entanglement detection and beyond.

Acknowledgments. This project was supported by the National Science Center (NCN), Poland, under Projects: Sonata Bis 10, No. 2020/38/E/ST3/00269 (L.P.)

Disclosure of Interests. The authors have no competing interests to declare that are relevant to the content of this article.

References

1. Bennett, C.H., DiVincenzo, D.P., Mor, T., Shor, P.W., Smolin, J.A., Terhal, B.M.: Unextendible product bases and bound entanglement. *Physical Review Letters* **82**(26), 5385–5388 (1999). <https://doi.org/10.1103/PhysRevLett.82.5385>
2. Cholewa, M., Gawron, P., Głomb, P., Kurzyk, D.: Quantum hidden Markov models based on transition operation matrices. *Quantum Information Processing* **16**(4), 101 (Mar 2017). <https://doi.org/10.1007/s11128-017-1544-8>
3. Cramer, M., Plenio, M.B., Flammia, S.T., Somma, R., Gross, D., Bartlett, S.D., Landon-Cardinal, O., Poulin, D., Liu, Y.K.: Efficient quantum state tomography. *Nature Communications* **1**(1), 149 (2010). <https://doi.org/10.1038/ncomms1147>
4. Devlin, J., Chang, M.W., Lee, K., Toutanova, K.: Bert: Pre-training of deep bidirectional transformers for language understanding (2019), <https://arxiv.org/abs/1810.04805>
5. Gawron, P., Kurzyk, D., Pawela, Ł.: QuantumInformation.jl—a julia package for numerical computation in quantum information theory. *PLOS ONE* **13**(12), e0209358 (dec 2018). <https://doi.org/10.1371/journal.pone.0209358>
6. Gisin, N., Thew, R.: Quantum communication. *Nature Photonics* **1**, 165–171 (2007). <https://doi.org/10.1038/nphoton.2007.22>
7. Goel, R., Xiao, Y., Ramezani, R.: Transformer models as an efficient replacement for statistical test suites to evaluate the quality of random numbers. In: 2024 International Symposium on Networks, Computers and Communications (ISNCC). pp. 1–6 (2024). <https://doi.org/10.1109/ISNCC62547.2024.10758985>
8. Goes, C.B.D., Canabarro, A., Duzzioni, E.I., Maciel, T.O.: Automated machine learning can classify bound entangled states with tomograms. *Quantum Information Processing* **20**(3), 99 (Mar 2021). <https://doi.org/10.1007/s11128-021-03037-9>
9. Greenwood, A.C., Wu, L.T., Zhu, E.Y., Kirby, B.T., Qian, L.: Machine-learning-derived entanglement witnesses. *Physical Review Applied* **19**(3), 034058 (2023). <https://doi.org/10.1103/PhysRevApplied.19.034058>
10. Gühne, O., Tóth, G.: Entanglement detection. *Physics Reports* **474**(1-6), 1–75 (2009). <https://doi.org/10.1016/j.physrep.2009.02.004>
11. Horodecki, M., Horodecki, P., Horodecki, R.: Separability of mixed states: necessary and sufficient conditions. *Physics Letters A* **223**(1-2), 1–8 (1996). [https://doi.org/10.1016/S0375-9601\(96\)00706-2](https://doi.org/10.1016/S0375-9601(96)00706-2)
12. Horodecki, P., Horodecki, M., Horodecki, R.: Mixed-state entanglement and distillation: is there a “bound” entanglement in nature? *Physical Review Letters* **80**(24), 5239–5242 (1998). <https://doi.org/10.1103/PhysRevLett.80.5239>
13. Horodecki, P., Horodecki, M., Horodecki, R.: Bound entanglement can be activated. *Physical Review Letters* **82**(5), 1056 (1999). <https://doi.org/10.1103/PhysRevLett.82.1056>
14. Horodecki, R., Horodecki, P., Horodecki, M., Horodecki, K.: Quantum entanglement. *Reviews of Modern Physics* **81**(2), 865–942 (2009). <https://doi.org/10.1103/RevModPhys.81.865>
15. Kukulski, R., Nechita, I., Pawela, Ł., Puchała, Z., Życzkowski, K.: Generating random quantum channels. *Journal of Mathematical Physics* **62**(6) (2021). <https://doi.org/10.1063/5.0038838>
16. Nielsen, M.A., Chuang, I.L.: *Quantum Computation and Quantum Information*. Cambridge University Press, 10th anniversary ed. edn. (2010)

17. Nielsen, M.A., Chuang, I.L.: Quantum computation and quantum information. Cambridge university press (2010)
18. Ozols, M.: How to generate a random unitary matrix. <http://home.lu.lv/sd20008> (2009), accessed: 2025-02-12
19. Peres, A.: Separability criterion for density matrices. *Physical Review Letters* **77**, 1413–1415 (1996). <https://doi.org/10.1103/PhysRevLett.77.1413>
20. Plenio, M.B., Virmani, S.: An introduction to entanglement measures. *Quantum Information & Computation* **7**(1-2), 1–51 (2007). <https://doi.org/10.5555/2011706.2011707>
21. Puchała, Z., Jenčová, A., Sedlák, M., Ziman, M.: Exploring boundaries of quantum convex structures: Special role of unitary processes. *Physical Review A* **92**, 012304 (2015). <https://doi.org/10.1103/PhysRevA.92.012304>
22. Śmierzchalski, T., Paweła, Ł., Puchała, Z., Trzciński, T., Gardas, B.: Post-error correction for quantum annealing processor using reinforcement learning. In: Groen, D., de Mulatier, C., Paszynski, M., Krzhizhanovskaya, V.V., Dongarra, J.J., Sloot, P.M.A. (eds.) *Computational Science – ICCS 2022*. pp. 261–268. Springer International Publishing (2022)
23. Vaswani, A., Shazeer, N., Parmar, N., Uszkoreit, J., Jones, L., Gomez, A.N., Kaiser, L.u., Polosukhin, I.: Attention is all you need. In: Guyon, I., Luxburg, U.V., Bengio, S., Wallach, H., Fergus, R., Vishwanathan, S., Garnett, R. (eds.) *Advances in Neural Information Processing Systems*. vol. 30. Curran Associates, Inc. (2017), https://proceedings.neurips.cc/paper_files/paper/2017/file/3f5ee243547dee91fbd053c1c4a845aa-Paper.pdf
24. Vidal, G., Werner, R.F.: A computable measure of entanglement. *Physical Review A* **65**(3), 032314 (2002). <https://doi.org/10.1103/PhysRevA.65.032314>
25. Watrous, J.: The theory of quantum information. Cambridge university press (2018)
26. Życzkowski, K.: Volume of the set of separable states. ii. *Physical Review A* **60**(5), 3496 (1999). <https://doi.org/10.1103/PhysRevA.60.3496>
27. Życzkowski, K., Horodecki, P., Sanpera, A., Lewenstein, M.: On the volume of the set of mixed entangled states. *Physical Review A* **58**(arXiv: quant-ph/9804024), 883 (1998). <https://doi.org/10.1103/PhysRevA.58.883>
28. Życzkowski, K., Horodecki, P., Sanpera, A., Lewenstein, M.: Volume of the set of separable states. *Physical Review A* **58**(2), 883 (1998). <https://doi.org/10.1103/PhysRevA.58.883>